Article

Structure

Structural insights into the bifunctional enzyme human FAD synthase

Graphical abstract

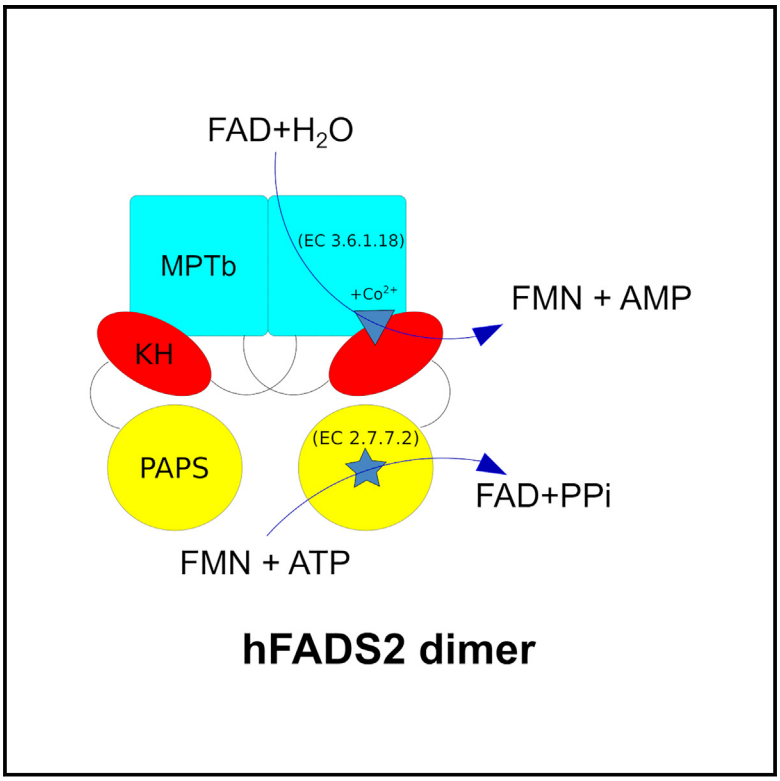

Highlights

- Crystal structures of the bifunctional enzyme hFADS2 were determined
- hFADS2 forms a stable C2-symmetric dimer involving the N-ter MPTb and KH domains
- The N-terminal MPTb and KH domains are essential for FAD hydrolysis

Authors

Giulia Leo, Piero Leone, Elham Ataie Kachoie, ..., Cesare Indiveri, Maria Barile, Stefano Capaldi

Correspondence

maria.barile@uniba.it (M.B.), stefano.capaldi@univr.it (S.C.)

In brief

Leo et al. report the crystal structures of the full-length protein and the C-terminal domain of human FADS2. Functional characterization revealed that hFADS2 is a bifunctional enzyme responsible for both FAD formation and degradation that are catalyzed by different domains. The degradation activity requires the dimeric form of the protein.

Leo et al., 2024, Structure *32*, 953–965
July 11, 2024
https://doi.org/10.1016/j.str.2024.04.006

CellPress

Structure

CellPress
OPEN ACCESS

Article

Structural insights into the bifunctional enzyme human FAD synthase

Giulia Leo,[1,5] Piero Leone,[2,5] Elham Ataie Kachoie,[1] Maria Tolomeo,[2,3] Michele Galluccio,[3] Cesare Indiveri,[3,4] Maria Barile,[2,*] and Stefano Capaldi[1,6,*]

[1]Department of Biotechnology, University of Verona, Strada Le Grazie 15, 37134 Verona, Italy
[2]Department of Biosciences, Biotechnology and Environment, University of Bari, via Orabona 4, 70126 Bari, Italy
[3]Department of Biology, Ecology and Earth Sciences (DiBEST), Laboratory of Biochemistry, Molecular Biotechnology, and Molecular Biology, University of Calabria, via P. Bucci 4c, 6c, 87036 Arcavacata di Rende, Italy
[4]National Research Council (CNR), Institute of Biomembranes, Bioenergetics and Molecular Biotechnologies (IBIOM), via Amendola 122/O, 70126 Bari, Italy
[5]These authors contribute equally
[6]Lead contact
*Correspondence: maria.barile@uniba.it (M.B.), stefano.capaldi@univr.it (S.C.)
https://doi.org/10.1016/j.str.2024.04.006

SUMMARY

Human flavin adenine dinucleotide synthase (hFADS) is a bifunctional, multi-domain enzyme that exhibits both flavin mononucleotide adenylyltransferase and pyrophosphatase activities. Here we report the crystal structure of full-length hFADS2 and its C-terminal PAPS domain in complex with flavin adenine dinucleotide (FAD), and dissect the structural determinants underlying the contribution of each individual domain, within isoforms 1 and 2, to each of the two enzymatic activities. Structural and functional characterization performed on complete or truncated constructs confirmed that the C-terminal domain tightly binds FAD and catalyzes its synthesis, while the combination of the N-terminal molybdopterin-binding and KH domains is the minimal essential substructure required for the hydrolysis of FAD and other ADP-containing dinucleotides. hFADS2 associates in a stable C2-symmetric dimer, in which the packing of the KH domain of one protomer against the N-terminal domain of the other creates the adenosine-specific active site responsible for the hydrolytic activity.

INTRODUCTION

Riboflavin (Rf), or vitamin B2, is an essential dietary component for humans and mammals, and its deficiency has been linked to several diseases, such as cancer, cardiovascular disease, anemia, abnormal fetal development, and various neuromuscular and neurological disorders, some of which are treatable with high doses of Rf.[1–5] The function of this vitamin in cell metabolism relies on its conversion to flavin mononucleotide (FMN) and flavin adenine dinucleotide (FAD), which are the redox cofactors for numerous dehydrogenases, reductases, and oxidases that exist in various subcellular compartments. They are crucial in many cellular processes, such as energy production, redox homeostasis, protein folding, apoptosis, and chromatin remodeling.[4,6,7] Given the importance of maintaining a functional flavoproteome in living cells, it is crucial to provide a clearer description of the molecular events responsible for the regulation and realization of Rf-derived cofactor homeostasis in human cells. Equally noteworthy is the intricate process of assembly of flavin cofactors to nascent flavoproteins and subsequent degradation during holoprotein turn-over.

In this scenario, a central role is played by FAD synthase (FADS), or rather ATP:FMN adenylyl transferase (FMNAT) (EC 2.7.7.2), i.e., the enzyme that adenylates FMN to FAD, catalyzing the last step of FAD biosynthesis from Rf,[8] which in humans is the product of the *FLAD1* gene.[9] *FLAD1* has been identified as the human orthologue of the first eukaryotic gene encoding for FADS discovered in *S. cerevisiae* and named *FAD1*.[10] Fad1p, the only known protein isoform generated from the *FAD1* gene of *S. cerevisiae*, even if in different echoforms,[11] is a 35.5 kDa soluble enzyme essential for yeast life, whose crystal structure has been solved in a complex with FAD bound in the active site.[12] Fad1p is a single-domain, monofunctional enzyme belonging to the 3′-phosphoadenosine 5′-phosphosulphate (PAPS) reductase family and shows little or no sequence similarity to prokaryotic FAD-forming enzymes.[13–16]

The relevance of *FLAD1* emerged in 2016, when *FLAD1* was identified as a novel disease gene of Rf-responsive multiple acyl-CoA dehydrogenation deficiency (MADD),[17] now identified as LSMFLAD (OMIM #255100), a heterogeneous class of lipid storage myopathies associated with altered fatty acid, amino acid, and choline metabolisms.[18,19] More recently, the potential of *FLAD1* products as biomarkers for cancer diagnosis and

prognosis has been highlighted.[20,21] Using pancreatic ductal adenocarcinoma cell lines (PDAC), Nisco et al. found that tumor parenchymal cells and the cancer stem cells (CSCs) generated from them express and activate FADS more frequently than normal cells. This observation encouraged the development of inhibitors as scaffolds for anti-cancer drugs, with Chicago Sky blue as a possible candidate.[22]

The human *FLAD1* gene, located on chromosome 1 at 1q21.3, encodes for FADS polypeptides of different sizes that are related to different transcript variants produced by alternative splicing of the gene. Isoforms 1 and 2 of human FAD synthase (hFADS1 and hFADS2) have been extensively studied by our group.[9,23–25] hFADS1 (GenBank Accession no: NM_025207.5) is a 587 amino acid (aa) protein with a predicted molecular mass of 65.3 kDa, whose first 17 residues contain a putative mitochondrial-targeting peptide;[23] hFADS2 (GenBank Accession no.: NM_201398.3), lacking the first 97 aa in the N-terminal region, is a protein of 490 residues with a predicted molecular mass of 54.2 kDa with cytosolic localization, and it is the most abundant isoform in the tissues/cells analyzed so far. Recent studies on muscle disorders[17] led to the identification of an additional, shorter isoform (hFADS6), which has been characterized in detail.[26]

Recombinant hFADS2 has been overexpressed, purified and its catalytic activity extensively characterized: FAD synthesis occurs via a bi-bi-mechanism in which ATP binds before FMN and pyrophosphate is released first, while the release of the cofactor, which remains tightly bound to the enzyme, to the client apoflavoprotein is the limiting step in the entire catalytic cycle.[25,27] hFADS2 also contains 10 cysteines, some of which appear to be redox-sensitive, suggesting its potential role as redox-sensor.[28]

hFADS2 is structurally organized in two domains, the C-terminal 3-phosphoadenosine 5′-phosphosulphate reductase (PAPS) domain (IPR002500), having FADS activity,[29,30] which is fused with an N-terminal molybdopterin-binding (MPTb) domain (IPR001453), whose function has remained unclear for many years since the identification of *FLAD1*. Further studies on recombinant hFADS2 finally revealed another important function of this protein, namely its cobalt-dependent, NON-NUDIX (nucleoside diphosphatase linked to X moiety) FAD hydrolase activity (EC 3.6.1.18) hidden in its N-terminal domain.[31,32] This activity, similar to that observed in prokaryotic enzymes containing a molybdopterin-like (MPTb) domain,[33] has also been observed in the monofunctional Fpy1p hydrolase of *S. cerevisiae*,[34] which has recently been shown to act as a NON-NUDIX pyrophosphatase toward FAD and NAD(H) (nicotinamide adenine dinucleotide).[35] It is not yet known whether the N-terminal domain is capable of FAD hydrolysis by itself, since no construct purified to date contains the MPTb domain alone. In this study we addressed this point by creating appropriate constructs containing either the MPTb domain alone or this domain fused with a hitherto undescribed intermediate domain, the dissection of which as a separate domain appears in the FADS structure predicted by AlphaFold.[36]

Homology modeling of human FADS domains have been performed,[26,32] but so far, no structural information on the complete protein is available. In the present study, we report the crystal structure of the entire hFADS2 and its C-terminal PAPS domain in complex with FAD, providing the molecular basis for elucidating its catalytic activities.

RESULTS

Protein expression and purification

On the basis of sequence homology, the five constructs, designed to express different combinations of hFADS domains, were selected for expression: $hFADS_{110-276}$ (MPTb), $hFADS_{110-354}$ (MPTb-KH domain), $hFADS_{355-553}$ (PAPS), $hFADS_{355-587}$ (PAPS-C-ter), and $hFADS_{110-587}$ (MPTb-KH-PAPS-C-ter), according to the numbering of the FADS isoform 1, Uniprot code Q8NFF5-1 (Figure S1A) were designed and produced as described in the STAR Methods section. The proteins overexpressed in *E. coli* and purified by Ni-chelating chromatography showed electrophoretic mobility consistent with theoretical molecular weight predicted by ProtParam tool (https://web.expasy.org/protparam/): ~55 kDa for $hFADS_{110-587}$ and ~22 kDa, ~27 kDa, ~18 kDa for $hFADS_{355-553}$, $hFADS_{355-587}$, and $hFADS_{110-276}$, respectively (Figure S1B). While all other constructs showed a single homogeneous band, fractions of $hFADS_{110-354}$ eluted with 250 mM imidazole showed two main bands migrating at about 25 and 23 kDa (Figure S1C). This result suggested that these purified protein fractions might be composed of two polypeptides of different sizes, possibly due to degradation processes during purification or some hydrolytic activity in the cells, or that the electrophoretic mobility of the protein might be influenced by the redox conditions. To verify the second hypothesis, the purified protein fraction was loaded and separated by SDS-PAGE in the presence or absence of dithiothreitol (DTT) (Figure S1C'), but no significant changes in the electrophoretic mobility were observed under different redox conditions. Immunoblotting experiments revealed that both bands display immunoreactivity with the anti-FADS antibody, indicating that both polypeptides correspond to hFADS fragments instead of co-eluting contaminants (Figure S1C'').

The overexpressed proteins were then characterized by spectrophotometric analysis. The spectra of the purified protein fractions are shown in Figure S1D. All proteins showed an absorbance peak at 274 nm, and as expected, only $hFADS_{110-587}$, $hFADS_{355-587}$, and $hFADS_{355-553}$ showed two additional minor peaks at 350 and 450 nm, which are typical for flavin-bound proteins. From the absorbance values at 280 and 450 nm, a FAD/protein monomer ratio of about 0.8 was calculated, as reported in a study by Leone et al.,[26] for the three constructs, indicating that they tightly bind FAD as observed with native hFADS2. The other two proteins, $hFADS_{110-276}$ and $hFADS_{110-354}$, lacking the PAPS domain, are unable to bind to endogenous FAD with high affinity and showed no other peaks in the visible region.

Kinetic properties of hFADS constructs

The purified hFADS constructs underwent kinetic characterization to investigate whether there were any variations or similarities in substrate interaction among themselves or compared to the previously characterized hFADS2 and hFADS6.[25,26,30,31] To test whether hFADS overexpressed recombinant constructs were capable of synthesizing or hydrolyzing FAD, purified proteins were incubated at room temperature with substrates, in

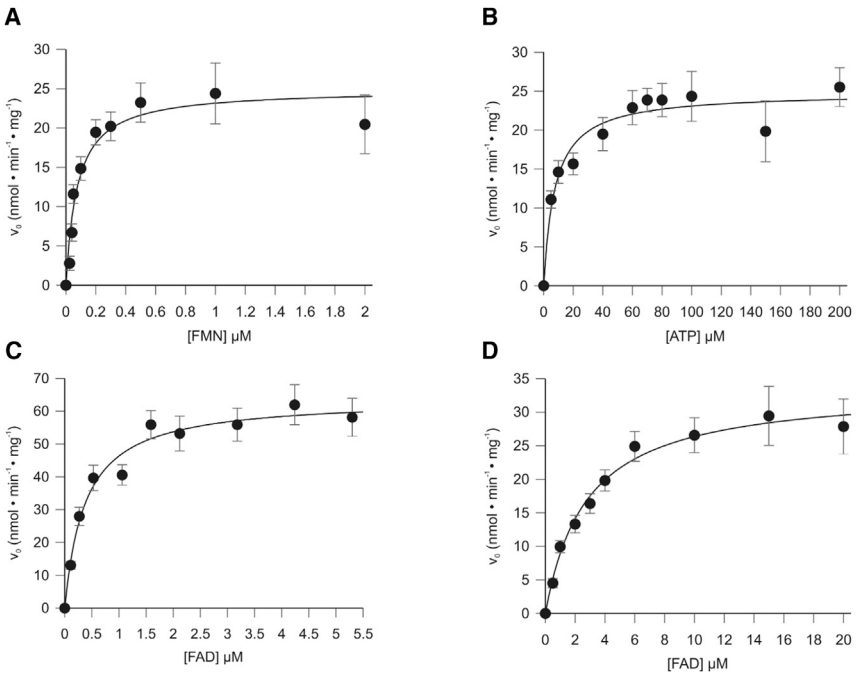

Figure 1. Kinetic properties of hFADS constructs

(A and B) FMN concentration dependence (A) and ATP concentration dependence (B) on FAD synthesis catalyzed by $hFADS_{110-587}$. The reaction was started by the addition of purified recombinant protein and measured by the initial rate of fluorescence decrease (λ ex = 450 nm, λ em = 520 nm). V_0 was measured as nmol · min^{-1} · mg^{-1}; data points are fitted according to the Michaelis-Menten equation with Grafit 5.0.13 software.

(C and D) FAD concentration dependence on FAD hydrolysis catalyzed by $hFADS_{110-587}$ (C) and $hFADS_{110-354}$ (D). FAD hydrolysis rate was measured by the initial rate of fluorescence increase (λ ex = 450 nm, λ em = 520 nm) in the presence of 1 mM $CoCl_2$, 50 mM KCl, and of the given FAD concentrations. The reported values are means ± SD from two independent experiments.

the absence or presence of Mg^{2+}, or Co^{2+} and K^+ for synthesis and hydrolysis, respectively, which are specifically required by native hFADS.[9,24–26] The FAD synthesis reaction, initiated by the addition of purified protein to ATP (100 µM) and FMN (2 µM), was followed by the decrease in fluorescence due to the conversion of the highly fluorescent FMN to the less fluorescent FAD. In contrast, hydrolysis of FAD was followed/displayed by increased fluorescence (λ ex = 450 nm, λ em = 520 nm) following FMN formation.

As shown in Figure S2A, $hFADS_{110-587}$ is able to promote FAD synthesis. This activity, which resides in the PAPS domain, is magnesium-dependent, as previously demonstrated for native hFADS isoforms.[9,24,25] In addition, this protein has the ability to catalyze the hydrolysis of FAD, an activity that is located in the MPTb domain and is cobalt-dependent (Figure S2B). Therefore, this construct behaves similarly to bifunctional hFADS2.[27,31]

Next, the dependence of the rate of FAD synthesis on the concentrations of the main substrates, FMN and ATP, was studied for the $hFADS_{110-587}$ construct in the presence of a saturating concentration of the counter-substrate, i.e., ATP and FMN, respectively (Figures 1A and 1B). The Km for FMN and ATP were calculated in 0.1 ± 0.05 µM and 7.6 ± 1.9 µM, respectively (Table S2). The Vmax was 25.9 ± 1.3 nmol · min^{-1} · mg^{-1} protein, corresponding to a kcat of 2.4 ± 0.1 · 10^{-2} s^{-1}. Comparing these data with those of native hFADS2, despite a lower kcat, lower Km values for the substrates suggested a possible higher affinity for this N-terminal truncated protein. Similar behavior was observed when the hydrolysis of FAD was measured by studying the dependence of the reaction rate on the FAD concentration (Figure 1C). The resulting Km was 0.4 ± 0.1 µM, and the Vmax value was 63.9 ± 2.4 nmol · min^{-1} · mg^{-1} protein, corresponding to a kcat of 5.9 ± 0.2 · 10^{-2} s^{-1}. Again, the kinetic characteristics indicated a higher affinity for this construct than for hFADS2.[31]

Purified $hFADS_{355-587}$, lacking the N-terminal domain and consisting only of the PAPS domain, catalyzes the synthesis but not the hydrolysis of FAD as expected (Figure S2A). From a kinetic point of view, this single-domain FADS construct showed similar behavior to that observed with the isolated PAPS domain or with hFADS6.[26,29] Remarkably, the $hFADS_{355-553}$ construct, lacking the last 34 residues, is not active at all, suggesting that the C-terminal portion of the protein is essential for FAD synthase activity.

The construct $hFADS_{110-276}$, comprising only the MPTb domain, showed no FAD synthesis activity, as expected. Notably, this protein also showed no FAD hydrolysis activity under any of the experimental conditions tested. In contrast, in the hFADS110-354 construct, consisting of the MPTb bound to the intermediate domain, the cobalt-dependent FAD hydrolysis activity was restored whereas, as expected given the absence of the PAPS domain, no synthesis activity was observed (Figure S2). The analysis of FAD hydrolysis rate of $hFADS_{110-354}$ revealed a saturating kinetic dependence on substrate concentration (Figure 1D). The Km for FAD was determined to be 2.8 ± 0.3 µM with a Vmax of 33.7 ± 1.2 nmol · min^{-1} · mg^{-1} protein, corresponding to a kcat of 1.6 ± 0.1 · 10^{-2} s^{-1}. These results indicate a decreased substrate affinity for $hFADS_{110-354}$ compared to the native hFADS2 isoform (Table S2). These results provide the first evidence that the combination of MPTb with the intermediate domain is the minimum essential substructure capable of carrying out FAD hydrolysis.

Overall structure of human FAD synthase

Despite numerous attempts with different constructs, we were only able to obtain moderately diffracting crystals of the entire hFADS2 with a construct lacking the first 12 residues ($hFADS_{110-587}$) in apo form. The crystals are monoclinic, space group $P2_1$, and exhibit high diffraction anisotropy, with the strongest diffraction along the a* axis. The structure was solved by molecular replacement combining two different search models corresponding to the predicted protein domains, and refined to a maximum resolution of 2.6 Å (R 21.5, R_{free} 26.8) with good

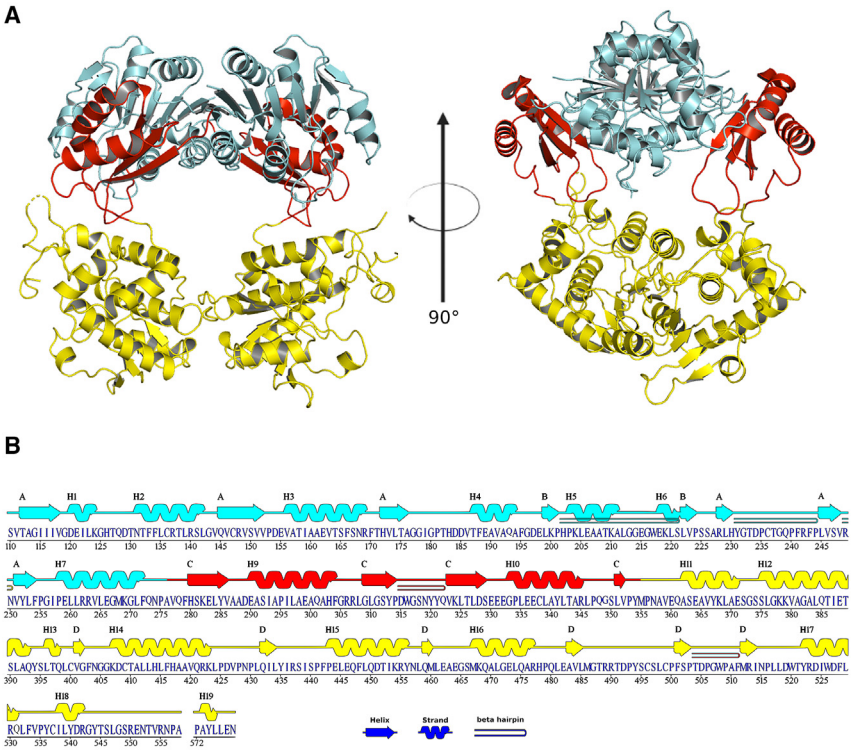

Figure 2. Structure of hFADS2 dimer

(A) Two orthogonal views of the hFADS2 dimer. The MPTb, KH, and PAPS domains are shown in light blue, red, and yellow, respectively.

(B) Amino acid sequence of a $hFADS_{110-587}$ protomer. The elements of the secondary structure are shown above with the same color code as (A). See also Figure S3.

stereochemistry (98% of the residues in the most favorable region of the Ramachandran plot with no outliers, Clashscore [Molprobity] 4.44) (Table 1).

The asymmetrical unit comprises four hFADS protomers (28,820 non-hydrogen atoms) assembled into two almost identical dimers (Figure 2A). Each protomer is composed of an N-terminal MPTb domain, an intermediate domain, and a C-terminal PAPS reductase (PAPS) domain (Figure S3A). The MPTb domain, spanning residues S110–P275, belongs to the MoaB/Mog family (also identified as COG1058 in the Clusters of Orthologous Groups database[37] and it shares 15% identity with the N-terminal domain of human gephyrin. The structure exhibits the classical folding pattern of the family, with three and two α-helices respectively packed on opposite sides of a parallel-antiparallel β-sheet composed of six β-strands. The intermediate domain (aa S280–V352, hereafter called KH domain) adopts a type I KH-like fold, with only two α-helices packed against one side of a 3-stranded β-sheet. The PAPS domain runs from residue N357 to P535, and displays the canonical fold of the HUP superfamily (CATHdb 3.40.50.620): a Rossman-like six-stranded (five parallel and one antiparallel) β-sheet faced by a single α-helix (H16) on one side and a bundle of five helices on the other.[38] An additional C-terminal "cap," spanning residues I538–T587 and composed of two short stretches of α-helices connected by long loops, extends over the catalytic active cavity of the protein. In this region, the solvent-exposed loop, which spans approximately residues 560–570, does not show a clear electronic density in all four protein molecules of the asymmetrical unit and was therefore not modeled. The secondary structure elements identified with Promotif[39] are displayed above the protein sequence in Figure 2B.

Two hFADS protomers tightly associate to form the dimeric biological form of the enzyme.[26,28] The dimer has C2 symmetry in which all domains are related by a common 2-fold symmetry axis (Figure S3B). The main contacts between the two monomers involve the N-terminal region of the protein, with interactions between the MPTb domains and the KH-like domain of one protomer packing against the MPTb of the other. Other minor contacts are established by the PAPS domains, in particular with the loops connecting helix H12 to the first β-strand and helix H14 to the second. A calculation performed with PISA[40] indicated a rather stable assembly, with a buried surface of 5480 $Å^2$ and 4870 $Å^2$ (ΔG^{diss} 27.1 kcal/mol and 17.5 kcal/mol) for dimers AB and CD, respectively (Figure S3C). When globally superimposed on each other by secondary-structure matching (SSM),[41] the two dimers in the asymmetric unit show an average root-mean-square deviation (RMSD) on Cα of 1.03 Å, but this value drops to 0.42 Å when the superimposition takes into account only the MPTb-KH-like domains (Figure S3D), indicating a higher structural rigidity of this part of the dimer, while the PAPS domains adopt a slightly different reciprocal orientation in the two assemblies. In addition, in each dimer, one of the PAPS domains (protomers A and C) is less tightly packed in the crystal lattice, resulting in higher average B-factors (Figure S3E) and a generally less defined electronic density map (Figure S3F). Overall, these observations suggest a quaternary structure in which the linkers connecting PAPS to the KH domain appear to be somewhat flexible, allowing the C-terminal domains more flexibility than the rigid N-terminal MPTb-KH dimer.

Structure of PAPS reductase domain in complex with FAD

In humans, FADS2 is responsible for the last step of FAD cofactor synthesis in the cytoplasm by catalyzing the adenylation of FMN via its C-terminal PAPS domain.[25,29] The product remains tightly bound to the enzyme active site, suggesting a feedback regulation of the enzymatic activity.[25,42] When recombinantly expressed, the isolated PAPS domain retains its binding and catalytic properties,[29] in accordance with the recent identification of a new isoform of FADS (hFADS6) lacking the N-terminal domain but still active in catalyzing FAD synthesis.[26]

Since we could not obtain diffraction-quality crystals of the full-length, product-bound protein, we expressed and crystallized

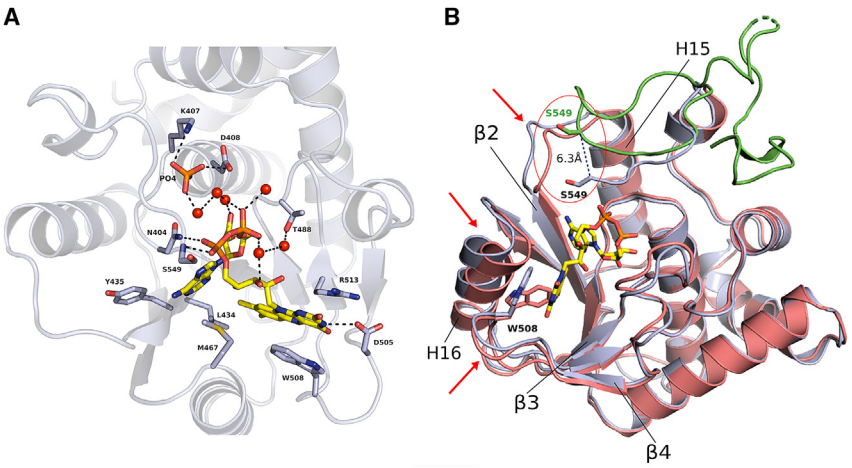

Figure 3. FAD binding to the FMNAT active site

(A) Details of the catalytic active site of the PAPS domain in complex with FAD and phosphate. The side chain of residues interacting with the ligands is displayed as sticks, water molecules are shown as red spheres. Hydrogen bonds are depicted as dashed lines.

(B) Superposition of FAD-bound (pink) with the apo PAPS domain (gray). The C-terminal "cap," absent in the construct crystallized in complex with FAD, is shown in green. The regions that exhibit the greatest conformational changes are indicated by the red arrows and the position of S549 in the two structures is highlighted with a red circle.

the isolated PAPS domain ($hFADS_{355-553}$) in complex with FAD. The crystals are orthorhombic (space group I222) and diffract to a maximum resolution of 1.69 Å. The structure was solved by molecular replacement and refined to an R_{free} of 20.7. The final model contains a single protein chain in the asymmetric unit, one FAD molecule, two phosphate ions and 136 water molecules (Table 1).

The clear electronic density of FAD and a phosphate ion (present in high concentration in the crystallization solution) allowed unambiguous modeling of the ligands in the active cavity of the PAPS domain (Figure S4A). As in yeast FAD synthases, FAD binds to the active cavity of the PAPS domain in a bent conformation, with the flavin and adenine moieties deeply buried into the binding cleft and the ribosyl-pyrophosphate group more exposed to the solvent.[12,43] The adenine ring fits into a hydrophobic pocket surrounded by the side chains of two residues in the second β-strand (Y435 and I436) and the side chains of N404 and M467, and is held in place by a hydrogen bond between N6 of adenine and the carbonyl group of I436. The isoalloxazine ring binds almost perpendicularly to the adenine moiety in the groove of the highly conserved "flavin motif" spanning residues D505–R513, with the plane of the ring parallel to the indole of W508 and the guanidinium group of R513. The carboxylate of D505 is hydrogen-bonded with N3 of the pyrimidine ring, blocking the reaction product at the active site and preventing its release. In fact, mutation of this residue has been shown to result in weaker binding to FAD and, in turn, an increased turnover rate of enzyme due to attenuation of product inhibition.[30,44] Other relevant interactions are a hydrogen bond between the carbonyl oxygen of G402 and O2 of ribose and between N of S549 and the β-phosphate. An extensive network of hydrogen bonds through water molecules connects the two phosphate groups to the protein backbone and side chains (Figure 3A).

A phosphate ion is clearly visible in the binding pocket at about 6.7 Å from the α-phosphate of FAD, hydrogen-bonded to the side chains of three residues of the PP-loop highly conserved in the PAPS reductase family[29,45]: K407, D408 and, through a water molecule, N404. It also interacts with the hydroxyl group of Y540 and main chain nitrogen of L547. The ion superimposes almost perfectly with a sulfate ion in the structure of *S. cerevisiae* Fad1p in complex with FAD (PDB ID: 2WSI),[12] and corresponds to the position of the ATP γ-phosphate in the ATP-bound *C. glabrata* FMNT (PDB ID: 3G59).[43]

The synthase activity of human FADS is strongly inhibited by thiol-blocking reagents such as mersalyl[28] or $HgCl_2$ (Figure S4B). The PAPS domain contains five reduced cysteine residues, and two of these, C400 and C409, are located in close proximity of the active site (Figure S4C). Although they are not directly involved in the proposed catalytic mechanism, their reaction with bulky metal groups can lead to a steric hindrance that blocks substrate binding, thus explaining the reduction in enzymatic activity. Two other cysteines (C496 and C499) are accessible and exposed to the solvent. Even though the crystals were obtained in the presence of a reducing agent (TCEP), it cannot be excluded that these residues may be available to form intermolecular disulfide bonds in non-reducing environments, in agreement with what was previously reported with the protein in solution.[28]

The PAPS domain bound to FAD aligns with the structure of the apo protein, with an overall Cα RMSD of 0.61 A (Figures 3B and S4D). This indicates that only minor conformational changes occur upon ligand binding. The main shifts involve helix 16 and the loop connecting the second β-strand with helix 15, which shift outward about 2.5 Å to enlarge the binding cavity (the calculated volume increases from 2601 to 2945 $Å^3$) and accommodate the ligand. Other minor changes are observed in the movement of the long loop connecting strands 3 and 4 and in the reorientation of the side chain of W508. Although the C-terminal "cap" (in green in Figure 3B) is not present in the structure of the $hFADS_{355-553}$– FAD complex, the position of the last visible residue, S549, much closer and hydrogen bonded to the pyrophosphate of the ligand, led us to speculate that this part of the protein may also undergo a reorientation that causes it to sit on top of and partially close the binding cavity. Notably, the absence of this C-terminal portion, which contains the highly conserved ARG2 motif (E582-R586), while not affecting the strong affinity of the PAPS domain for the reaction product, renders this construct totally inactive (Figure S2A). In this regard, it is most likely that the catalytic activity of hFADS2 depends largely on the interaction between the Arg side chains of the ARG2 motif and the phosphate groups of the incoming substrates.

Structural basis of adenine dinucleotide pyrophosphatase activity of hFADS

Human FADS has been shown to be a bifunctional enzyme that, in addition to the well-characterized FMN adenylyltransferase, also displays pyrophosphatase activity toward adenine dinucleotides, including its own product, FAD. In fact, hFADS promotes the hydrolysis of the pyrophosphate bond in FAD and NADH by a NON NUDIX mechanism in the presence of K^+ and some divalent cations, with Co^{2+} exhibiting the highest efficiency.[31] This adenine dinucleotide pyrophosphatase (ADPP) activity is absent in the isolated PAPS domain, indicating that the N-terminal region of the protein is indeed responsible for this additional enzymatic property.[32]

Both FAD and NAD(H) possess a common ADP moiety, while the rest of the molecule differs in size and chemical nature (Figure 4A). This suggests the presence of a substrate recognition mechanism, whereby the adenine nucleotide selectively binds to an active site within the N-terminal region of the protein. To investigate this hypothesis, we conducted isothermal titration calorimetry (ITC) measurements using different nucleotides on the isolated MPTb domain in solution (Figure 4B; Table S3). ATP and ADP bind to MPTb in an approximately 1:1 M ratio, although their affinity is relatively low (Kd values between 200 and 250 μM). ADP-ribose and NADH exhibit a slightly higher affinity, with Kd values between 50 and 100 μM, while FAD displays the highest affinity for the protein domain. It is important to note, however, that a strong exothermic contribution during each injection, possibly due to the ligand's heat of dilution, may have resulted in a less accurate estimate of the binding heats during this experiment. Interestingly, no binding was observed with GTP, which is consistent with previous findings that showed GTP (and other non-adenine nucleotides) has a reduced ability to inhibit FAD hydrolysis (as reported in a study by Leone et al.[31]). These results confirm the presence of an adenosine-specific binding site within the N-terminal domain of hFADS, which can explain its selectivity in the hydrolytic degradation of adenine-containing dinucleotides. However, the MPTb domain alone ($hFADS_{110-276}$) did not exhibit any activity when tested in the FAD hydrolysis assay (Figure S2B). On the other hand, the $hFADS_{110-354}$ construct, comprising the MPTb and KH domains, showed considerable catalytic activity, similar to that observed in the entire protein (Figures 1D and S2B). These observations support a model in which the hydrolytic active site of hFADS is located in the large cleft of MPTb near the interface between the two domains (Figure S5A), but one or more residues in the KH domain are required for catalytic activity.

As shown in Figure 2C, in the hFADS dimer each KH domain interacts with the MPTb domain of the other protomer, and this dimeric structure of the protein is therefore essential for its hydrolytic activity. Notably, a residual electron density in the Fo-Fc map is present in this cavity in all the four protomers in the asymmetric unit of the apo protein structure (Figure S5B). The size and position of the aforementioned density, surrounded by the side chain carboxylates of four acidic residues, are consistent with the presence of a Mg-water cluster, albeit not included in the model due to the suboptimal resolution of the structure. It is worth noting that the magnesium ion bound to pyrophosphate occupies a similar position in the ligand bound structures of *T. thermophilus* competence-induced protein (CinA),[46] a prokaryotic enzyme with ADP-ribose pyrophosphatase activity and structurally analogous to human FADS in its N-terminal portion (see Discussion).

Despite extensive search, we were unable to obtain diffracting crystals of hFADS in complex with any ligand, so we relied on *in silico* molecular docking to characterize substrate binding in the hydrolytic active site. Three independent blind docking experiments were performed on a complete $hFADS_{110-587}$ dimer using ADP-ribose, FAD, and NADH, generating a total of 27 separate poses for each ligand ranked according to the free energy of binding. Remarkably, the 15 top-scoring poses identified the binding site in the cleft described previously for all ligands, with only one exception in the case of FAD which was also docked in the PAPS domain (Figures S5C–S5E). The best predicted binding mode (i.e., the one with the lowest energy) for each substrate is shown in Figures 5A–5C. In all cases, the ligand fits into the cavity in a similar orientation. The adenine ring is inserted into a hydrophobic pocket surrounded by the side chains of residues situated in the loops connecting the first and second helices (P256–P258) and the sixth β-strand to the seventh helix of the MPTb domain (T127–N131), and in the second strand of the KH domain (Y313–W316). Comparison of the three structures revealed a near-perfect overlap of the adenosine-pyrophosphate moiety of the substrates, while the remaining part of the molecule adopts a distinct conformation within the larger pocket on the opposite side of the binding cavity (Figure 5D).

Taken together, these findings establish a molecular basis underlying the specificity of hFADS2 toward ADP-containing dinucleotides.

DISCUSSION

Isoform 2 of FAD synthase is responsible for the cytosolic production of the essential cofactor FAD in humans through the condensation of ATP and FMN. It is a multi-domain, bifunctional enzyme that couples the synthetic function with a hydrolytic activity toward adenosine dinucleotides.[31,32]

The crystal structure of the recombinant protein revealed that hFADS2 is a physiological dimer, consistent with previous findings for the homologue extracted from rat liver.[47,48] The two protomers closely associate to form a quaternary C2-symmetrical structure, primarily through interactions between the N-terminal MPTb and KH domains. Each monomer also includes a PAPS domain at the C-terminus, which catalyses FAD synthesis independently. The latter displays a high degree of structural homology with the yeast orthologues FMN adenylyl transferase (FMNAT) from *C. glabrata*[43] and Fad1 from *S. cerevisiae*.[12] Unlike their mammalian counterparts, yeast FAD synthases are single-domain, monofunctional proteins with only synthase activity. Although they share a rather low sequence identity (~23%) with the PAPS domain of human FADS2 (Figure 6A), the overall folding and structural motifs involved in substrate binding remained well conserved during evolution. A structural comparison between the PAPS domain of apo hFADS2 and *Cg*FMNAT revealed a good degree of overlap of the secondary structure elements, with an overall RMSD of ~1.5 Å (Figure 6B). The main differences concern the orientation of the first helix α1, which in hFADS2 is bound to the upstream KH domain, and the structure of the C-terminal region, where the extended

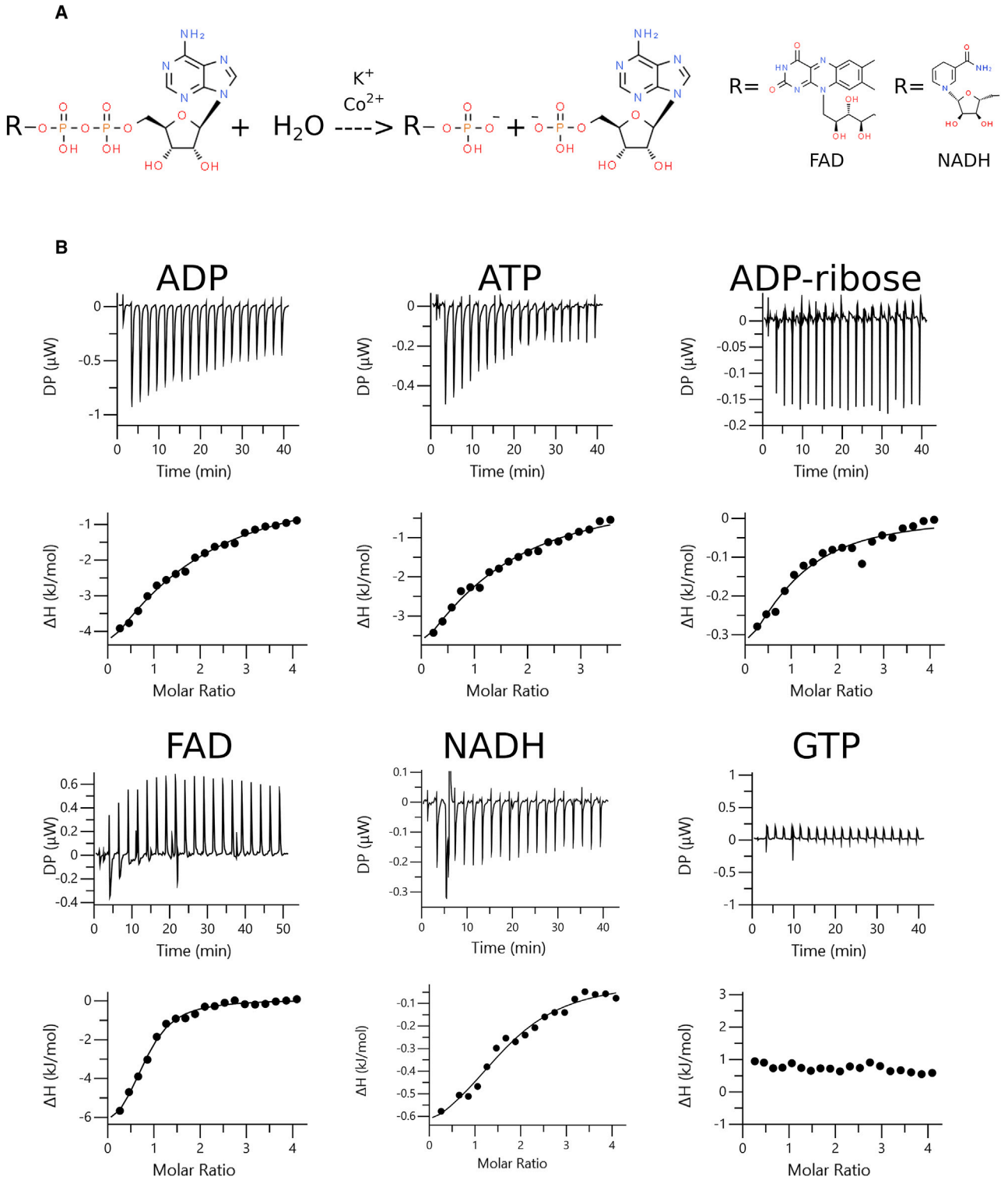

Figure 4. Substrate specificity of the ADPP active site

(A) Schematic representation of adenine dinucleotides hydrolysis reaction.

(B) ITC analysis of the MPTb domain binding to various nucleotides. Upper panels: raw ITC data, lower panels: corrected integrated heats as function of the molar ratio. The thermodynamic binding parameters for each ligand are reported in Table S1.

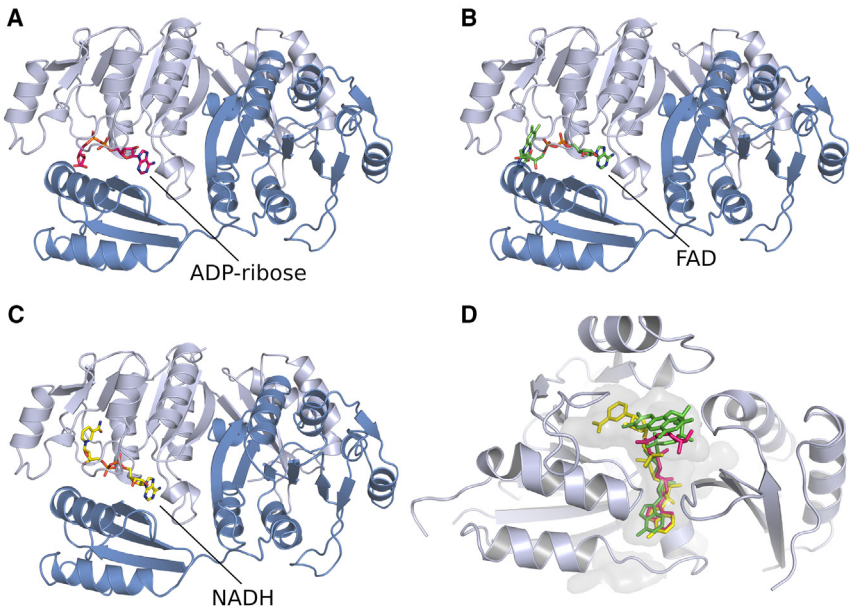

Figure 5. Substrates docking to the ADPP active site of hFADS2

(A–C) The docking pose with the highest score for ADP-ribose (A, pink), FAD (B, green), and NADH (C, yellow) on an hFADS2 dimer. For better visualization, only the MPTb-KH domains are shown.

(D) Superposition of the three docked substrates. The binding cavity is represented by the gray surface. See also Figure S5.

loop containing helices 8 and 9 of the yeast orthologue is absent in the human enzyme. These differences, however, do not seem to have an impact on substrate binding and catalytic activity in the three proteins. In fact, similar values have been reported for the steady-state kinetic parameters of *C. glabrata* FMNAT and human FADS2. A structural comparison of the binding mode reveals an almost perfect overlap of the flavin and adenine moieties of FAD in the three proteins, while greater variability is observed for the position of the pyrophosphate group (Figure 6C). This reflects the different conformation of the flexible ARG1 loop, which in hFADS2 occupies an intermediate position between the "closed" and "open" conformation observed in *Cg*FMNAT and *Sc*FAD1, respectively. Finally, in all three structures a negative ion (phosphate or sulfate) is tightly bound in the position occupied by the γ-phosphate of ATP before the adenylation reaction, hydrogen-bonded to the highly conserved Lys residue of the PP-loop.

Human FADS2 is a bifunctional enzyme that, in addition to FAD synthase activity, also displays pyrophosphatase activity toward dinucleotide cofactors such as FAD and NAD(H) in its N-terminal

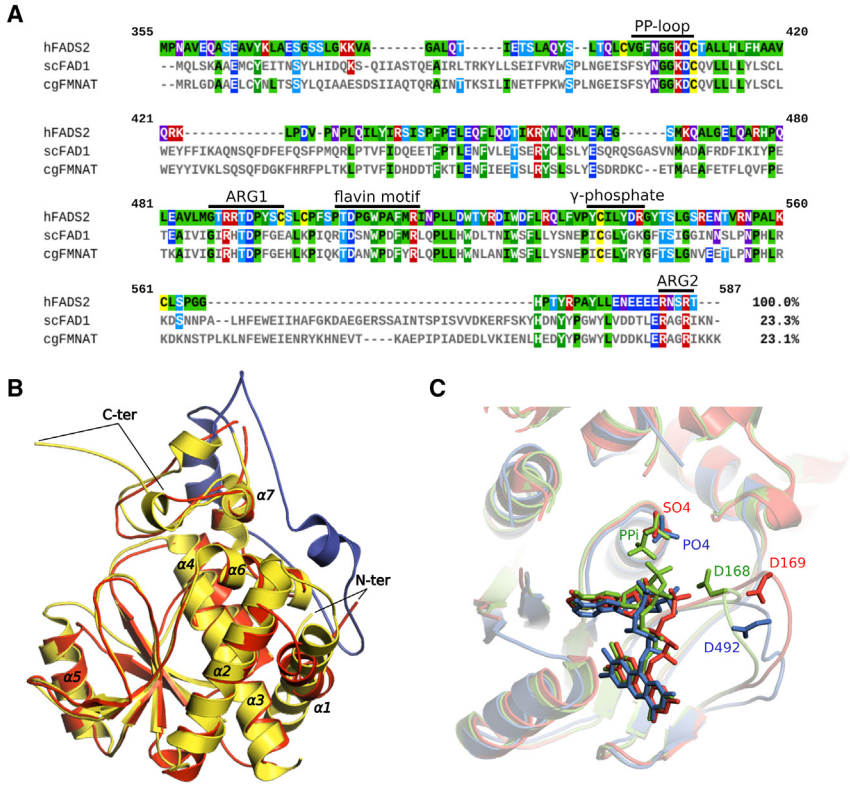

Figure 6. Structural homology of hFADS2 PAPS domain with yeast orthologues

(A) Sequence alignment of human FADS2 (hFADS2) with *Candida glabrata* flavin mononucleotide adenylyltransferase (*Cg*FMNAT) and *Saccharomyces cerevisiae* FAD synthetase (*Sc*FAD1). Conserved residues are highlighted (green, hydrophobic; dark green, large hydrophobic; red, positive charge; blue, negative charge; light blue, small alcohol; yellow, cysteine; purple, polar) and the percentage of identity with hFADS2 is reported for each protein. The conserved motifs involved in ligand binding are indicated above the sequence.

(B) Superposed cartoon models of apo hFADS2 PAPS domain (yellow) and apo *Cg*FMNAT (3FWK, red). The C-terminal helix-loop-helix motif of the yeast protein, absent in human FADS2, is colored in blue.

(C) FAD binding in hFADS2 (blue), *Cg*FMNAT (3FWK, green), and ScFAD1 (2WSI, red). The ligands and negatively charged ions in the active site are represented as stick models. The side chain of the conserved Asp residue of the ARG1 loop is shown in all three structures.

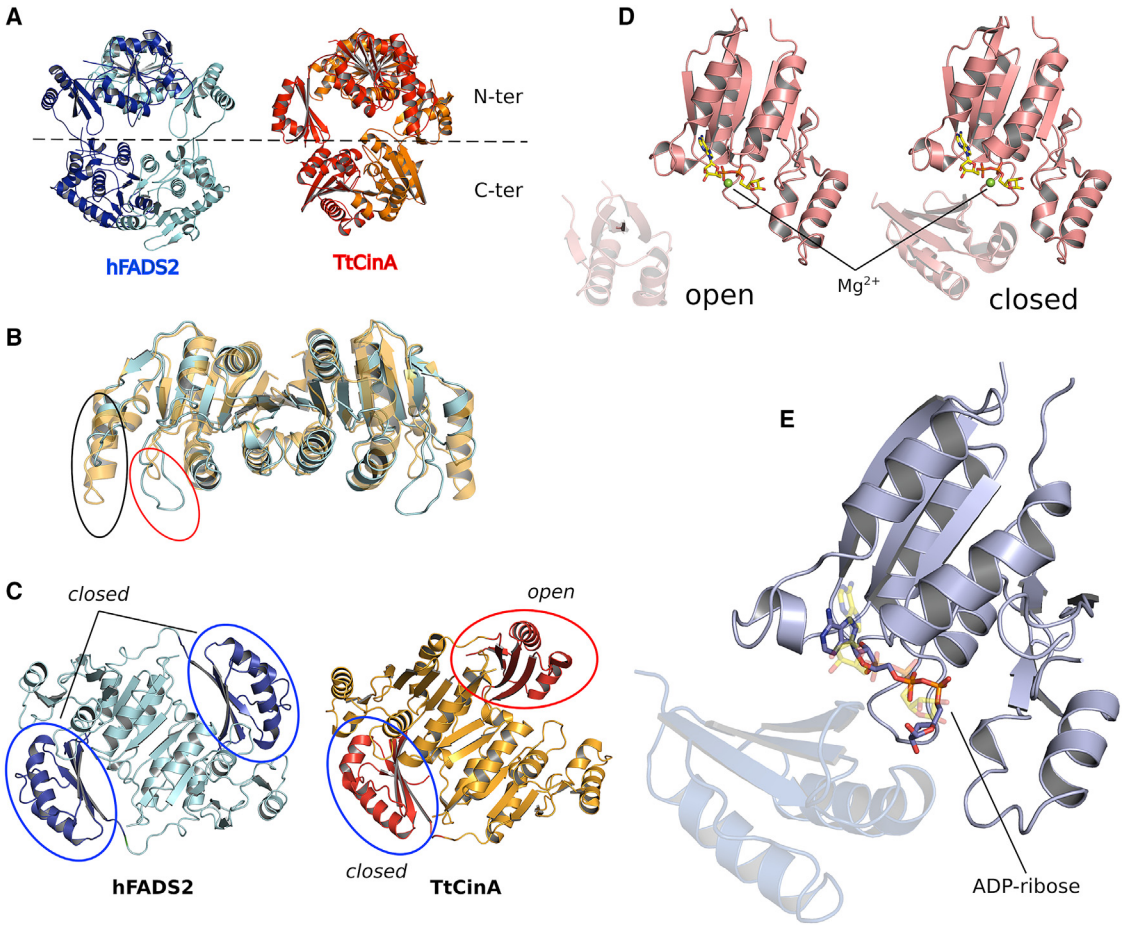

Figure 7. Comparison of hFADS2 and the prokaryotic bifunctional enzyme *Tt*CinA

(A) Ribbon representation of the hFADS2 (blue) and *T. termophilus* CinA (4CT8, red) dimers with approximately the same orientation of the MPTb domains.

(B) Overlay of the MPTb dimeric substructure of hFADS (light blue) and *Tt*CinA (gold, 4CT8). Regions showing significant structural changes in the first and second β-hairpin are highlighted by a black and red oval, respectively.

(C) The orientation of the KH domains in hFADS2 (blue) and in *Tt*CinA (red) dimers. Both KH domains are in the "closed" conformation (blue circles), while one is in the "open" conformation in *Tt*CinA (red circle).

(D) ADP-ribose bound to the "open" (left) and "closed" (right) binding site of *Tt*CinA (4UUX). The ligand is shown in stick and Mg^{2+} atoms as green spheres.

(E) The best docking pose for ADP-ribose on hFADS2. For comparison, the conformation of ADP-ribose bound to the "closed" site of superimposed *Tt*CinA (yellow sticks) is shown in transparency.

MPTb-KH domains.[31,32] This hydrolytic activity is similar to that described on ADP-ribose in other prokaryotic enzymes containing an MPTb (or COG1058) domain, such as *S. oneidensis* NMN deamidase (PncC)[33] or the CinA from *Thermus thermophilus*, whose crystal structure was determined a few years ago.[46] Similar to hFADS2, *Tt*CinA is also a bifunctional, dimeric enzyme in which a MPTb-KH substructure is fused with a C-terminal NMN deamidase domain (Figure 7A). The MPTb domains of the two proteins have approximately 36% sequence identity and share a high degree of structure similarity (Cα RMSD <2.2 Å), with the main differences being in the two β-hairpin motifs connecting strands 4–5 and 6–7, respectively (Figure 7B). There is, however, a remarkable difference in the organization of the dimer in CinA: it shows an asymmetric arrangement in which one of the KH domains is packed against the other protomer, similar to hFADS2, while the other is rotated outwards, in an "open" conformation in which it makes no contact with the MPTb of the opposite monomer (Figure 7C). ADP-ribose has been shown to bind to CinA, in a complex with an Mg^{2+} ion, in both the open and the closed sites in an almost identical conformation (Figure 7D). The best docking pose obtained on hFADS2 is also very similar in position and orientation, with the pyrophosphate group that nearly overlaps that of CinA, and the adenine ring slightly rotated and less buried into the cavity (Figure 7E). While ADP-ribose fits completely into the binding site in both proteins, it is worth noting that in hFADS2, the loop of the second β-hairpin adopts an open conformation, creating a large space on the other side of the binding cavity to accommodate the isoalloxazine or nicotinamide groups of FAD and NADH (Figure S6), which would instead be sterically hindered by binding to CinA in the same way. The asymmetric nature of CinA led the authors to hypothesize a catalytic cycle in which the two MPTb domains alternate between the open and closed conformations. The substrate (ADP-ribose), initially bound in the open site, is brought into the closed active site by a rotation of the MPTb dimer relative to the

Table 1. Structure determination statistics

Dataset	$hFADS_{355-553}$–FAD complex	$hFADS_{110-587}$
Space group	I222	P21
a (Å)	63.96	75.75
b (Å)	69.73	187.74
c (Å)	105.33	79.38
α (°)	90.0	90.0
β (°)	90.0	96.45
γ (°)	90.0	90.0
Resolution Range (Å)	58.14–1.69	58.72–2.49
Observed reflections	106004	291040
Independent reflections	24610	43831
Rmerge	0.063 (0.746)	0.124 (1.312)
Rpim	0.033 (0.416)	0.052 (0.533)
Mean I/sd(I)	8.3 (2.3)	9.8 (1.5)
Completeness (%)	92.1 (99.7)	–
Completeness (ellipsoidal)[a] (%)	–	93.2 (71.3)
CC(1/2)	0.996 (0.649)	0.996 (0.485)
Reflections in refinement	24597	43432
Rcryst.	18.3	21.5
Rfree (test set 5%)	20.7	26.8
Protein atoms (no hydrogen)	1674	14498
Ligand atoms (no hydrogen)	58	–
Water molecules	136	–
r.m.s.d. on bond lengths (Å)	0.011	0.008
r.m.s.d. on bond angles (°)	1.192	0.824
Average B factor - protein ($Å^2$)	33.75	75.99
Average B factor - ligands ($Å^2$)	27.72	–
Average B factor - water ($Å^2$)	40.55	–

The values in parentheses refer to the highest resolution shell, i.e., 1.72–1.69 Å for the PAPS domain – FAD complex dataset, and 2.79–2.49 Å for the apo MPTb-KH-C-ter dataset.
[a]As determined by anisotropic data analysis with STARANISO.

rest of the molecule, where residues of the adjacent KH domain participate in the catalytic process.[46] In the case of hFADS2, both sites are simultaneously in the closed (active) conformation, and the symmetrical structure of the dimer does not suggest a mechanism similar to that of CinA. In this case, it is most likely that the substrate binds to the site already in the active state and the products are released without major structural changes.

The ADP-ribose pyrophosphatase activity of prokaryotic proteins containing the MPTb domain, including *Tt*CinA, is highly dependent on the presence of Co^{2+} and K^+, with other divalent metal ions (Mn^{2+} and Ni^{2+}) being able to partially replace cobalt albeit less efficiently.[33] hFADS2 also shows similar metal-dependent, NON-NUDIX activity for hydrolysis of FAD and NADH.[31] Co^{2+} shows significantly higher efficiency than the other cations, and the activity is enhanced by the presence of thiol-blocking agents, such as mersalyl.[32] While the presence of an Mg^{2+} ion in the active site seems to be important for substrate binding, as also inferred from the structures of CinA in complex with ADPR and ATP, the role of Co^{2+} in the catalytic process remains unclear. The lack of canonical high-affinity metal-binding motifs in hFADS2, together with the extremely low levels of free Co^{2+} in the cytoplasm, makes it difficult to establish its involvement in the catalytic mechanism and to hypothesize a strong constitutive hydrolytic activity for this enzyme under physiological conditions. On the other hand, the known effect of CoCl2 in inducing chemical hypoxia in cultured cells[49] suggests that hFADS2 may respond, by regulating the rate of hydrolysis and turnover of FAD (and possibly NAD(H)), to hypoxic conditions due to increased concentrations of free metal ions (Co^{2+}, but also Ni^{2+} and Mn^{2+}) within the cell.

In conclusion, human FADS is one of the very few examples of an enzyme with two distinct active sites that perform different and opposite catalytic activities, the synthesis and hydrolysis of FAD, respectively. In this study, we presented the crystal structure of the entire enzyme and its synthase domain in complex with the reaction product. The biological assembly consists of a dimer in which two independent PAPS domains, responsible for FAD synthesis, are linked to a symmetrical dimeric structure formed by the interaction of the MPTb and KH domains. Each of the two hydrolytic active sites is located in a pocket of MPTb at the interface with the KH domain of the other protomer, which is essential for catalytic activity.

Although further studies are needed to fully elucidate the molecular mechanisms regulating the catalytic activities of human FADS, our results represent a significant advance in the understanding of the function of this enzyme and its role in dinucleotide redox cofactor homeostasis.

STAR★METHODS

Detailed methods are provided in the online version of this paper and include the following:

- KEY RESOURCES TABLE
- RESOURCE AVAILABILITY
  - Lead contact
  - Materials availability
  - Data and code availability
- EXPERIMENTAL MODEL AND STUDY PARTICIPANT DETAILS
  - Cloning and recombinant protein production
- METHOD DETAILS
  - Protein expression and purification
  - Immunoblotting
  - Protein concentration and FAD/protein monomer ratio measurements
  - Crystallization and X-Ray structure determination
  - Isothermal titration Calorimetry (ITC)
  - Measurements of FAD synthesis and FAD hydrolysis
  - Molecular docking
- QUANTIFICATION AND STATISTICAL ANALYSIS

SUPPLEMENTAL INFORMATION

Supplemental information can be found online at https://doi.org/10.1016/j.str.2024.04.006.

ACKNOWLEDGMENTS

We are grateful to the staff of the ESRF synchrotron in Grenoble (Proposal MX 2464) for assistance during data collection. We acknowledge "Centro Piattaforme Tecnologiche" of the University of Verona for giving access to ITC and mass spectrometry instrumentation. Piero Leone is recipient of a research fellowship funded by PNRR Project CN00000041 "National Center for Gene Therapy and Drugs based on RNA technology". This work was also supported by the European Union - NextGenerationEU through the Italian Ministry of University and Research under PNRR - M4C2-I1.3 Project PE_00000019 "HEAL ITALIA" to S.C.

AUTHOR CONTRIBUTIONS

Conceptualization, M.B., C.I., and S.C.; investigation, G.L., P.L, E.A.K., M.T., and M.G.; writing – original draft, S.C.; writing – review & editing, P.L, M.G., M.B., C.I., and S.C.; funding acquisition, M.B. and S.C.; supervision, M.B. and S.C.

DECLARATION OF INTERESTS

The authors declare no competing interests.

Received: February 8, 2024
Revised: March 20, 2024
Accepted: April 3, 2024
Published: April 29, 2024

REFERENCES

1. Gregersen, N. (1985). Riboflavin-responsive defects of beta-oxidation. J. Inherit. Metab. Dis. *8* (*Suppl 1*), 65–69. https://doi.org/10.1007/BF01800662.
2. Powers, H.J. (2003). Riboflavin (vitamin B-2) and health. Am. J. Clin. Nutr. *77*, 1352–1360. https://doi.org/10.1093/ajcn/77.6.1352.
3. Nakano, E., Mushtaq, S., Heath, P.R., Lee, E.-S., Bury, J.P., Riley, S.A., Powers, H.J., and Corfe, B.M. (2011). Riboflavin depletion impairs cell proliferation in adult human duodenum: identification of potential effectors. Dig. Dis. Sci. *56*, 1007–1019. https://doi.org/10.1007/s10620-010-1374-3.
4. Barile, M., Giancaspero, T.A., Leone, P., Galluccio, M., and Indiveri, C. (2016). Riboflavin transport and metabolism in humans. J. Inherit. Metab. Dis. *39*, 545–557. https://doi.org/10.1007/s10545-016-9950-0.
5. Tolomeo, M., Nisco, A., Leone, P., and Barile, M. (2020). Development of Novel Experimental Models to Study Flavoproteome Alterations in Human Neuromuscular Diseases: The Effect of Rf Therapy. Int. J. Mol. Sci. *21*, 5310. https://doi.org/10.3390/ijms21155310.
6. Joosten, V., and van Berkel, W.J.H. (2007). Flavoenzymes. Curr. Opin. Chem. Biol. *11*, 195–202. https://doi.org/10.1016/j.cbpa.2007.01.010.
7. Hino, S., Sakamoto, A., Nagaoka, K., Anan, K., Wang, Y., Mimasu, S., Umehara, T., Yokoyama, S., Kosai, K.-I., and Nakao, M. (2012). FAD-dependent lysine-specific demethylase-1 regulates cellular energy expenditure. Nat. Commun. *3*, 758. https://doi.org/10.1038/ncomms1755.
8. McCormick, D.B., and Zhang, Z. (1993). Cellular assimilation of water-soluble vitamins in the mammal: riboflavin, B6, biotin, and C. Proc. Soc. Exp. Biol. Med. *202*, 265–270. https://doi.org/10.3181/00379727-202-43534b.
9. Brizio, C., Galluccio, M., Wait, R., Torchetti, E.M., Bafunno, V., Accardi, R., Gianazza, E., Indiveri, C., and Barile, M. (2006). Over-expression in Escherichia coli and characterization of two recombinant isoforms of human FAD synthetase. Biochem. Biophys. Res. Commun. *344*, 1008–1016. https://doi.org/10.1016/j.bbrc.2006.04.003.
10. Wu, M., Repetto, B., Glerum, D.M., and Tzagoloff, A. (1995). Cloning and characterization of FAD1, the structural gene for flavin adenine dinucleotide synthetase of Saccharomyces cerevisiae. Mol. Cell. Biol. *15*, 264–271. https://doi.org/10.1128/MCB.15.1.264.
11. Bruni, F., Giancaspero, T.A., Oreb, M., Tolomeo, M., Leone, P., Boles, E., Roberti, M., Caselle, M., and Barile, M. (2021). Subcellular Localization of Fad1p in Saccharomyces cerevisiae: A Choice at Post-Transcriptional Level? Life *11*, 967. https://doi.org/10.3390/life11090967.
12. Leulliot, N., Blondeau, K., Keller, J., Ulryck, N., Quevillon-Cheruel, S., and Van Tilbeurgh, H. (2010). Crystal Structure of Yeast FAD Synthetase (Fad1) in Complex with FAD. J. Mol. Biol. *398*, 641–646. https://doi.org/10.1016/j.jmb.2010.03.040.
13. Frago, S., Martínez-Júlvez, M., Serrano, A., and Medina, M. (2008). Structural analysis of FAD synthetase from Corynebacterium ammoniagenes. BMC Microbiol. *8*, 160. https://doi.org/10.1186/1471-2180-8-160.
14. Herguedas, B., Martínez-Júlvez, M., Frago, S., Medina, M., and Hermoso, J.A. (2010). Oligomeric state in the crystal structure of modular FAD synthetase provides insights into its sequential catalysis in prokaryotes. J. Mol. Biol. *400*, 218–230. https://doi.org/10.1016/j.jmb.2010.05.018.
15. Serrano, A., Sebastián, M., Arilla-Luna, S., Baquedano, S., Pallarés, M.C., Lostao, A., Herguedas, B., Velázquez-Campoy, A., Martínez-Júlvez, M., and Medina, M. (2015). Quaternary organization in a bifunctional prokaryotic FAD synthetase: Involvement of an arginine at its adenylyltransferase module on the riboflavin kinase activity. Biochim. Biophys. Acta *1854*, 897–906. https://doi.org/10.1016/j.bbapap.2015.03.005.
16. Yatsyshyn, V.Y., Ishchuk, O.P., Voronovsky, A.Y., Fedorovych, D.V., and Sibirny, A.A. (2009). Production of flavin mononucleotide by metabolically engineered yeast Candida famata. Metab. Eng. *11*, 163–167. https://doi.org/10.1016/j.ymben.2009.01.004.
17. Olsen, R.K.J., Koňaříková, E., Giancaspero, T.A., Mosegaard, S., Boczonadi, V., Mataković, L., Veauville-Merllié, A., Terrile, C., Schwarzmayr, T., Haack, T.B., et al. (2016). Riboflavin-Responsive and -Non-responsive Mutations in FAD Synthase Cause Multiple Acyl-CoA Dehydrogenase and Combined Respiratory-Chain Deficiency. Am. J. Hum. Genet. *98*, 1130–1145. https://doi.org/10.1016/j.ajhg.2016.04.006.
18. Gregersen, N., Wintzensen, H., Christensen, S.K., Christensen, M.F., Brandt, N.J., and Rasmussen, K. (1982). C6-C10-dicarboxylic aciduria: investigations of a patient with riboflavin responsive multiple acyl-CoA dehydrogenation defects. Pediatr. Res. *16*, 861–868. https://doi.org/10.1203/00006450-198210000-00012.

19. Antozzi, C., Garavaglia, B., Mora, M., Rimoldi, M., Morandi, L., Ursino, E., and DiDonato, S. (1994). Late-onset riboflavin-responsive myopathy with combined multiple acyl coenzyme A dehydrogenase and respiratory chain deficiency. Neurology *44*, 2153–2158. https://doi.org/10.1212/wnl.44.11.2153.

20. Mei, M., Song, W., Wang, Y., and Zhang, M. (2021). Significant Diagnostic and Prognostic Value of FLAD1 and Related MicroRNAs in Breast Cancer after a Pan-Cancer Analysis. Dis. Markers *2021*, 6962526. https://doi.org/10.1155/2021/6962526.

21. Hu, P., Pan, Y., Wang, C., Zhang, W., Huang, H., Wang, J., and Zhang, N. (2020). FLAD1 is up-regulated in Gastric Cancer and is a potential prediction of prognosis. Int. J. Med. Sci. *17*, 1763–1772. https://doi.org/10.7150/ijms.48162.

22. Nisco, A., Carvalho, T.M.A., Tolomeo, M., Di Molfetta, D., Leone, P., Galluccio, M., Medina, M., Indiveri, C., Reshkin, S.J., Cardone, R.A., and Barile, M. (2023). Increased demand for FAD synthesis in differentiated and stem pancreatic cancer cells is accomplished by modulating FLAD1 gene expression: the inhibitory effect of Chicago Sky Blue. FEBS J. *290*, 4679–4694. https://doi.org/10.1111/febs.16881.

23. Torchetti, E.M., Brizio, C., Colella, M., Galluccio, M., Giancaspero, T.A., Indiveri, C., Roberti, M., and Barile, M. (2010). Mitochondrial localization of human FAD synthetase isoform 1. Mitochondrion *10*, 263–273. https://doi.org/10.1016/j.mito.2009.12.149.

24. Galluccio, M., Brizio, C., Torchetti, E.M., Ferranti, P., Gianazza, E., Indiveri, C., and Barile, M. (2007). Over-expression in Escherichia coli, purification and characterization of isoform 2 of human FAD synthetase. Protein Expr. Purif. *52*, 175–181. https://doi.org/10.1016/j.pep.2006.09.002.

25. Torchetti, E.M., Bonomi, F., Galluccio, M., Gianazza, E., Giancaspero, T.A., Iametti, S., Indiveri, C., and Barile, M. (2011). Human FAD synthase (isoform 2): a component of the machinery that delivers FAD to apo-flavoproteins: Isoform 2 of human FAD synthase. FEBS J. *278*, 4434–4449. https://doi.org/10.1111/j.1742-4658.2011.08368.x.

26. Leone, P., Galluccio, M., Barbiroli, A., Eberini, I., Tolomeo, M., Vrenna, F., Gianazza, E., Iametti, S., Bonomi, F., Indiveri, C., et al. (2018). Bacterial Production, Characterization and Protein Modeling of a Novel Monofuctional Isoform of FAD Synthase in Humans: An Emergency Protein? Molecules *23*, 116. https://doi.org/10.3390/molecules23010116.

27. Giancaspero, T.A., Colella, M., Brizio, C., Difonzo, G., Fiorino, G.M., Leone, P., Brandsch, R., Bonomi, F., Iametti, S., and Barile, M. (2015). Remaining challenges in cellular flavin cofactor homeostasis and flavoprotein biogenesis. Front. Chem. *3*, 30. https://doi.org/10.3389/fchem.2015.00030.

28. Miccolis, A., Galluccio, M., Nitride, C., Giancaspero, T.A., Ferranti, P., Iametti, S., Indiveri, C., Bonomi, F., and Barile, M. (2014). Significance of redox-active cysteines in human FAD synthase isoform 2. Biochim. Biophys. Acta Protein Proteomics *1844*, 2086–2095. https://doi.org/10.1016/j.bbapap.2014.08.005.

29. Miccolis, A., Galluccio, M., Giancaspero, T.A., Indiveri, C., and Barile, M. (2012). Bacterial Over-Expression and Purification of the 3'phosphoadenosine 5'phosphosulfate (PAPS) Reductase Domain of Human FAD Synthase: Functional Characterization and Homology Modeling. Int. J. Mol. Sci. *13*, 16880–16898. https://doi.org/10.3390/ijms131216880.

30. Leone, P., Galluccio, M., Quarta, S., Anoz-Carbonell, E., Medina, M., Indiveri, C., and Barile, M. (2019). Mutation of Aspartate 238 in FAD Synthase Isoform 6 Increases the Specific Activity by Weakening the FAD Binding. Int. J. Mol. Sci. *20*, 6203. https://doi.org/10.3390/ijms20246203.

31. Leone, P., Galluccio, M., Brizio, C., Barbiroli, A., Iametti, S., Indiveri, C., and Barile, M. (2019). The hidden side of the human FAD synthase 2. Int. J. Biol. Macromol. *138*, 986–995. https://doi.org/10.1016/j.ijbiomac.2019.07.138.

32. Giancaspero, T.A., Galluccio, M., Miccolis, A., Leone, P., Eberini, I., Iametti, S., Indiveri, C., and Barile, M. (2015). Human FAD synthase is a bi-functional enzyme with a FAD hydrolase activity in the molybdopterin binding domain. Biochem. Biophys. Res. Commun. *465*, 443–449. https://doi.org/10.1016/j.bbrc.2015.08.035.

33. Cialabrini, L., Ruggieri, S., Kazanov, M.D., Sorci, L., Mazzola, F., Orsomando, G., Osterman, A.L., and Raffaelli, N. (2013). Genomics-Guided Analysis of NAD Recycling Yields Functional Elucidation of COG1058 as a New Family of Pyrophosphatases. PLoS One *8*, e65595. https://doi.org/10.1371/journal.pone.0065595.

34. Pallotta, M.L. (2011). Evidence for the presence of a FAD pyrophosphatase and a FMN phosphohydrolase in yeast mitochondria: a possible role in flavin homeostasis. Yeast *28*, 693–705. https://doi.org/10.1002/yea.1897.

35. Lynch, J.H., Sa, N., Saeheng, S., Raffaelli, N., and Roje, S. (2018). Characterization of a non-nudix pyrophosphatase points to interplay between flavin and NAD(H) homeostasis in Saccharomyces cerevisiae. PLoS One *13*, e0198787. https://doi.org/10.1371/journal.pone.0198787.

36. Jumper, J., Evans, R., Pritzel, A., Green, T., Figurnov, M., Ronneberger, O., Tunyasuvunakool, K., Bates, R., Žídek, A., Potapenko, A., et al. (2021). Highly accurate protein structure prediction with AlphaFold. Nature *596*, 583–589. https://doi.org/10.1038/s41586-021-03819-2.

37. Tatusov, R.L., Natale, D.A., Garkavtsev, I.V., Tatusova, T.A., Shankavaram, U.T., Rao, B.S., Kiryutin, B., Galperin, M.Y., Fedorova, N.D., and Koonin, E.V. (2001). The COG database: new developments in phylogenetic classification of proteins from complete genomes. Nucleic Acids Res. *29*, 22–28. https://doi.org/10.1093/nar/29.1.22.

38. Aravind, L., Anantharaman, V., and Koonin, E.V. (2002). Monophyly of class I aminoacyl tRNA synthetase, USPA, ETFP, photolyase, and PP-ATPase nucleotide-binding domains: implications for protein evolution in the RNA world. Proteins *48*, 1–14. https://doi.org/10.1002/prot.10064.

39. Hutchinson, E.G., and Thornton, J.M. (1996). PROMOTIF-A program to identify and analyze structural motifs in proteins: Program to analyze protein structural motifs. Protein Sci. *5*, 212–220. https://doi.org/10.1002/pro.5560050204.

40. Krissinel, E., and Henrick, K. (2007). Inference of Macromolecular Assemblies from Crystalline State. J. Mol. Biol. *372*, 774–797. https://doi.org/10.1016/j.jmb.2007.05.022.

41. Krissinel, E., and Henrick, K. (2004). Secondary-structure matching (SSM), a new tool for fast protein structure alignment in three dimensions. Acta Crystallogr. D Biol. Crystallogr. *60*, 2256–2268. https://doi.org/10.1107/S0907444904026460.

42. Yamada, Y., Merrill, A.H., and McCormick, D.B. (1990). Probable reaction mechanisms of flavokinase and FAD synthetase from rat liver. Arch. Biochem. Biophys. *278*, 125–130. https://doi.org/10.1016/0003-9861(90)90240-y.

43. Huerta, C., Borek, D., Machius, M., Grishin, N.V., and Zhang, H. (2009). Structure and Mechanism of a Eukaryotic FMN Adenylyltransferase. J. Mol. Biol. *389*, 388–400. https://doi.org/10.1016/j.jmb.2009.04.022.

44. Huerta, C., Grishin, N.V., and Zhang, H. (2013). The "super mutant" of yeast FMN adenylyltransferase enhances the enzyme turnover rate by attenuating product inhibition. Biochemistry *52*, 3615–3617. https://doi.org/10.1021/bi400454w.

45. Bork, P., and Koonin, E.V. (1994). A P-loop-like motif in a widespread ATP pyrophosphatase domain: implications for the evolution of sequence motifs and enzyme activity. Proteins *20*, 347–355. https://doi.org/10.1002/prot.340200407.

46. Karuppiah, V., Thistlethwaite, A., Dajani, R., Warwicker, J., and Derrick, J.P. (2014). Structure and Mechanism of the Bifunctional CinA Enzyme from Thermus thermophilus. J. Biol. Chem. *289*, 33187–33197. https://doi.org/10.1074/jbc.M114.608448.

47. Oka, M., and McCormick, D.B. (1987). Complete purification and general characterization of FAD synthetase from rat liver. J. Biol. Chem. *262*, 7418–7422. https://doi.org/10.1016/S0021-9258(18)48253-1.

48. Barile, M., Brizio, C., Valenti, D., De Virgilio, C., and Passarella, S. (2000). The riboflavin/FAD cycle in rat liver mitochondria. Eur. J. Biochem. *267*, 4888–4900. https://doi.org/10.1046/j.1432-1327.2000.01552.x.

49. Muñoz-Sánchez, J., and Chánez-Cárdenas, M.E. (2019). The use of cobalt chloride as a chemical hypoxia model. J. Appl. Toxicol. *39*, 556–570. https://doi.org/10.1002/jat.3749.

50. Pettersen, E.F., Goddard, T.D., Huang, C.C., Couch, G.S., Greenblatt, D.M., Meng, E.C., and Ferrin, T.E. (2004). UCSF Chimera–a visualization system for exploratory research and analysis. J. Comput. Chem. *25*, 1605–1612. https://doi.org/10.1002/jcc.20084.

51. Trott, O., and Olson, A.J. (2010). AutoDock Vina: improving the speed and accuracy of docking with a new scoring function, efficient optimization, and multithreading. J. Comput. Chem. *31*, 455–461. https://doi.org/10.1002/jcc.21334.

52. Vonrhein, C., Flensburg, C., Keller, P., Sharff, A., Smart, O., Paciorek, W., Womack, T., and Bricogne, G. (2011). Data processing and analysis with the *autoPROC* toolbox. Acta Crystallogr. D Biol. Crystallogr. *67*, 293–302. https://doi.org/10.1107/S0907444911007773.

53. Tickle, I., Flensburg, C., Keller, P., Paciorek, W., Sharff, A., Vonrhein, C., and Bricogne, G. (2018). STARANISO. http://staraniso.globalphasing.org/cgi-bin/staraniso.cgi.

54. Vagin, A., and Teplyakov, A. (2010). Molecular replacement with *MOLREP*. Acta Crystallogr. D Biol. Crystallogr. *66*, 22–25. https://doi.org/10.1107/S0907444909042589.

55. Murshudov, G.N., Skubák, P., Lebedev, A.A., Pannu, N.S., Steiner, R.A., Nicholls, R.A., Winn, M.D., Long, F., and Vagin, A.A. (2011). *REFMAC* 5 for the refinement of macromolecular crystal structures. Acta Crystallogr. D Biol. Crystallogr. *67*, 355–367. https://doi.org/10.1107/S0907444911001314.

56. Liebschner, D., Afonine, P.V., Baker, M.L., Bunkóczi, G., Chen, V.B., Croll, T.I., Hintze, B., Hung, L.-W., Jain, S., McCoy, A.J., et al. (2019). Macromolecular structure determination using X-rays, neutrons and electrons: recent developments in *Phenix*. Acta Crystallogr. Sect. Struct. Biol. *75*, 861–877. https://doi.org/10.1107/S2059798319011471.

57. McCoy, A.J., Grosse-Kunstleve, R.W., Adams, P.D., Winn, M.D., Storoni, L.C., and Read, R.J. (2007). *Phaser* crystallographic software. J. Appl. Crystallogr. *40*, 658–674. https://doi.org/10.1107/S0021889807021206.

58. Terwilliger, T.C., Grosse-Kunstleve, R.W., Afonine, P.V., Moriarty, N.W., Zwart, P.H., Hung, L.-W., Read, R.J., and Adams, P.D. (2008). Iterative model building, structure refinement and density modification with the *PHENIX AutoBuild* wizard. Acta Crystallogr. D Biol. Crystallogr. *64*, 61–69. https://doi.org/10.1107/S090744490705024X.

59. Chen, V.B., Arendall, W.B., Headd, J.J., Keedy, D.A., Immormino, R.M., Kapral, G.J., Murray, L.W., Richardson, J.S., and Richardson, D.C. (2010). *MolProbity* : all-atom structure validation for macromolecular crystallography. Acta Crystallogr. D Biol. Crystallogr. *66*, 12–21. https://doi.org/10.1107/S0907444909042073.

60. Leone, P., Quarta, S., Tolomeo, M., and Barile, M. (2021). Purification of Recombinant Human 6His-FAD Synthase (Isoform 2) and Quantitation of FAD/Protein Monomer Ratio by UV-Vis Spectra. Methods Mol. Biol. *2280*, 69–85. https://doi.org/10.1007/978-1-0716-1286-6_6.

61. Emsley, P., Lohkamp, B., Scott, W.G., and Cowtan, K. (2010). Features and development of *Coot*. Acta Crystallogr. D Biol. Crystallogr. *66*, 486–501. https://doi.org/10.1107/S0907444910007493.

62. Leone, P., Tolomeo, M., and Barile, M. (2021). Continuous and Discontinuous Approaches to Study FAD Synthesis and Degradation Catalyzed by Purified Recombinant FAD Synthase or Cellular Fractions. Methods Mol. Biol. *2280*, 87–116. https://doi.org/10.1007/978-1-0716-1286-6_7.

63. Barile, M., Passarella, S., Bertoldi, A., and Quagliariello, E. (1993). Flavin adenine dinucleotide synthesis in isolated rat liver mitochondria caused by imported flavin mononucleotide. Arch. Biochem. Biophys. *305*, 442–447. https://doi.org/10.1006/abbi.1993.1444.

64. Barile, M., Brizio, C., De Virgilio, C., Delfine, S., Quagliariello, E., and Passarella, S. (1997). Flavin adenine dinucleotide and flavin mononucleotide metabolism in rat liver–the occurrence of FAD pyrophosphatase and FMN phosphohydrolase in isolated mitochondria. Eur. J. Biochem. *249*, 777–785. https://doi.org/10.1111/j.1432-1033.1997.00777.x.

65. Morris, G.M., Huey, R., Lindstrom, W., Sanner, M.F., Belew, R.K., Goodsell, D.S., and Olson, A.J. (2009). AutoDock4 and AutoDockTools4: Automated docking with selective receptor flexibility. J. Comput. Chem. *30*, 2785–2791. https://doi.org/10.1002/jcc.21256.

STAR★METHODS

KEY RESOURCES TABLE

REAGENT or RESOURCE	SOURCE	IDENTIFIER
Antibodies		
In-house produced polyclonal rabbit antiserum against hFADS	Biochemisty and molecular biology department, Università degli Studi di Bari "Aldo Moro" Biochemistry and molecular biotechnology unit, Università della Calabria	Patent n. WO2009107158 A1
Anti-rabbit immunoglobulin antibody, alkaline phosphatase conjugated	Merck	Cat#051M6180 A8025; RRID: AB_258372
Bacterial and virus strains		
Escherichia coli Rosetta (DE3)	Novagen	Cat#70954
Escherichia coli DH5α	Thermofisher	Cat#18265017
Chemicals, peptides, and recombinant proteins		
Acrylamide-Bis-acrylamide, 30% solution	Merck	Cat#A3574
ATP	Merck	Cat#A26209
BamHI restriction endonuclease	Jena Biosciences	Cat#EN-103S
BSA	Merck	Cat#A4503
$CoCl_2$	Merck	Cat#C2644
DMSO	Merck	Cat#D8418
DNAse	Merck	Cat#DN25
Ethylene glycol	Merck	Cat#102466
FAD	Merck	Cat#F6625
FMN	Merck	Cat#F2253
HEPES	Merck	Cat#H3375
Imidazole	Merck	Cat#I202
IPTG	Merck	Cat#I6758
KCl	Merck	Cat#P4504
MES	Merck	Cat#M5057
$MgCl_2$	Merck	Cat#0162
NaCl	Merck	Cat#S9625
NdeI restriction endonuclease	Jena Biosciences	Cat#EN-E229301
PEG4000	Merck	Cat#807490
PIC	Merck	Cat#P8849
PMSF	Merck	Cat#P7626
PVDF membrane	Millipore	Cat#IPVH00010
SDS	Merck	Cat#L3771
T4 DNA ligase	Jena Biosciences	Cat#EN-149S
TCEP	Merck	Cat#C4706
Thrombin	Merck	Cat#T4648
TRIS	Merck	Cat#T6066
Critical commercial assays		
GelElute Gel extraction Kit	Merck	Cat#NA1111
Dye reagent for protein assay	Bio-Rad	Cat#5000006
JCSG-plus crystalization kit	Molecular Dimensions	Cat#MD1-37
PACT premier crystalization kit	Molecular Dimensions	Cat#MD1-29
The LMB Crystallisation Screen	Molecular Dimensions	Cat#MD1-98

(*Continued on next page*)

Continued

REAGENT or RESOURCE	SOURCE	IDENTIFIER
Deposited data		
Crystal structure of human FAD synthase PAPS domain in complex with FAD	This paper	PDB: 8ROM
Crystal structure of human FAD synthase, isoform	This paper	PDB: 8RON
Candida glabrata FMN adenylyltransferase	Huerta et al.[43]	PDB: 3FWK
Crystal structure of yeast FAD Synthetase (Fad1) in Complex with FAD	Leulliot et al.[12]	PDB: 2WSI
Competence or damage-inducible protein CinA from Thermus thermophilus	Karuppiah et al.[46]	PDB ID: 4UUW
Competence or damage-inducible protein CinA from Thermus thermophilus	Karuppiah et al.[46]	PDB ID: 4UUX
Oligonucleotides		
FADS-ET15-110-f: GGTGGTCATATGAGCGTGACGGCT	This paper	N/A
FADS-ET15-277-f: GGTGGTCATATGGTTCAGTTCCAC	This paper	N/A
FADS-ET15-355-f: GGTGGTCATATGCCCAACGCTGTG	This paper	N/A
FADS-ET15-276-r: GGTGGTGGATCCTCAAGCTGGGTTTTG	This paper	N/A
FADS-ET15-354-r: GGTGGTGGATCCTCAGTAGGGGACCAG	This paper	N/A
FADS-ET15-553-r: GGTGGTGGATCCTCAGGTATTCTCCCG	This paper	N/A
FADS-ET15-587-r: GGTGGTGGATCCTCATGTGCGGGAGTT	This paper	N/A
Recombinant DNA		
pET15b vector	Novagen	Cat#69661-3
hFADS2-pH6EX3	Torchetti et al.[25]	N/A
$hFADS_{110-276}$-pET15b	This paper	N/A
$hFADS_{110-354}$-pET15b	This paper	N/A
$hFADS_{355-553}$-pET15b	This paper	N/A
$hFADS_{355-587}$-pET15b	This paper	N/A
$hFADS_{110-587}$-pET15b	This paper	N/A
Software and algorithms		
Grafit software v. 5.0.13	Erithacus Software	http://www.erithacus.com/grafit/grafit_5_service_pack.htm
ImageLab 6.0	Bio-rad	https://www.bio-rad.com/it-it/product/image-lab-software?ID=KRE6P5E8Z
Expasy ProtParam tool	Swiss Institute of Bioinformatics	https://web.expasy.org/protparam/protparam-doc.html
PubChem Database	National Center for Biotechnology Information	https://pubchem.ncbi.nlm.nih.gov/
Chimera v1.16	Pettersen et al.[50]	https://www.cgl.ucsf.edu/chimera/download.html
AutoDock Vina	Trott et al.[51]	https://autodock.scripps.edu/
autoPROC	Vonrhein et al.[52]	https://www.globalphasing.com/autoproc/
STARANISO server	Tickle et al.[53]	https://staraniso.globalphasing.org/cgi-bin/staraniso.cgi
MOLREP	Vagin et al.[54]	https://www.ccp4.ac.uk/
Refmac 5	Murshudov et al.[55]	https://www.ccp4.ac.uk/

(*Continued on next page*)

Continued

REAGENT or RESOURCE	SOURCE	IDENTIFIER
Phenix Refine	Liebschner et al.[56]	https://phenix-online.org/download
Phaser	McCoy et al.[57]	https://phenix-online.org/download https://www.ccp4.ac.uk/
Phenix Autobuild	Terwilliger et al.[58]	https://phenix-online.org/download
MolProbity	Chen et al.[59]	http://molprobity.biochem.duke.edu/
PyMOL	Schrödinger	http://www.pymol.org
Other		
Chelating Sepharose Fast Flow	Cytiva	Cat#17057501
Superdex 200 prep grade resin	Cytiva	Cat#17104301
Superdex 75 prep grade resin	Cytiva	Cat#17104401
FP-8300 spectrofluorometer	Jasco	N/A
MicroCal PEAQ-ITC	Malvern Panalyrical	N/A
Ultrospec 3100-Pro spectrophotometer	Amersham Biosciences	N/A
ID23-2 beamline	European Synchrotron Radiation Facility (ESRF)	N/A
ID30B beamline	European Synchrotron Radiation Facility (ESRF)	N/A

RESOURCE AVAILABILITY

Lead contact

Further information and requests for resources and reagents should be directed to and will be fulfilled by the lead contact, Stefano Capaldi (stefano.capaldi@univr.it).

Materials availability

Plasmids generated in this study will be made available upon request to the lead contact.

Data and code availability

- Coordinate and structure factor data for $hFADS_{110-587}$ in apo form and of the PAPS domain ($hFADS_{355-553}$) in complex with FAD have been deposited at Protein Data Bank with accession number 8RON and 8ROM, and are publicly available as of the date of publication.
- This paper does not report original code.
- Any additional information required to reanalyze the data reported in this paper is available from the lead contact upon request.

EXPERIMENTAL MODEL AND STUDY PARTICIPANT DETAILS

Cloning and recombinant protein production

E. coli DH5α competent cells were used for cloning and plasmid preparation. Rosetta *E. coli* strain was used for protein expression.

METHOD DETAILS

Protein expression and purification

The cDNA sequences of the different hFADS2 constructs were amplified by PCR using primers designed to introduce restriction sites for the endonucleases *Nde*I and *BamH*I. The amplicons were purified, digested and ligated into the pET15b vector, which introduces an N-terminal histidine tag and a thrombin cleavage site. The resulting recombinant vectors were used to transform Rosetta *E. coli* cells. The same protocol, adapted from the ones previously described[9,24,25,60] was used for the expression and purification of the different constructs. Briefly, cell cultures (1–2 L for each preparation) were grown at 37°C and gene expression was induced overnight at 20°C with 0.5 mM IPTG (isopropyl β- D -thiogalactopyranoside). Cells were collected by centrifugation, resuspended in HEPES 20 mM pH 7.5, 0.5 M NaCl, 20 mM imidazole, 0.5 mM TCEP, 5 mM $MgCl_2$, 20 μg/mL DNAse, 1 mM PMSF and sonicated 3 times for 30 s. To obtain FAD-saturated proteins, 20 μM FAD was added before sonication. The soluble fraction was collected by centrifugation and loaded onto a nickel-IDA Sepharose column equilibrated in HEPES 20 mM pH 7.5, 0.5 M NaCl, 20 mM imidazole, 0.5 mM TCEP. The column was extensively washed with the same buffer containing 50 mM imidazole and the bound protein was then eluted with 250 mM imidazole. The His-tag was removed by overnight digestion with thrombin and the proteins were further

purified by gel filtration on a Superdex 75 or Superdex 200 column equilibrated with 20 mM HEPES pH 7.5, 0.15 M NaCl and 0.5 mM TCEP. The purity of the final protein samples was checked by SDS-PAGE and immunoblotting.

Immunoblotting

SDS-PAGE-separated proteins were electro-transferred onto a nitrocellulose membrane using a *trans*-blot semidry electrophoretic transfer cell. The immobilized proteins were incubated for 3 h with a 3000-fold dilution of an in-house produced polyclonal antiserum against hFADSs. The bound antibody was visualized with the aid of a secondary anti-rabbit immunoglobulin antibody, conjugated with alkaline phosphatase (1:5000 dilution).

Protein concentration and FAD/protein monomer ratio measurements

Protein concentration was measured with the method of Bradford, using BSA as standard. In an alternative procedure, the protein concentration of the purified 6His-hFADS was estimated by absorbance spectra, which were recorded on an Ultrospec 3100 pro spectrophotometer, essentially as in.[25,60] To this aim, the contribution of the bound FAD had to be subtracted from the A280 readings. Because A280 for both free FAD and hFADS-bound FAD is 1.7-fold A450, the A280, actually due to the apo-protein, may be calculated from the Equation:

$$A_{280}\ apoenzyme\ =\ A_{280}\ -\ (A_{450}\ \times\ 1.7)$$

The protein concentration was then estimated by using ε280 for the different hFADS truncated proteins as calculated from the protein sequence by using the Expasy ProtParam tool (Swiss Institute of Bioinformatics, Lausanne, Switzerland). Measurements made by either the spectrophotometric or the Bradford method differed by no more than 7%. The FAD/protein monomer ratio (given as percent flavinylation, Fl%) could be estimated from the absorbance spectrum by considering:

$$Fl\%\ =\ [(A_{450}/A_{280}apoenzyme)/R]\ \times 100$$

where R is the ε450 FAD/ε280 apoenzyme ratio, as reported in Table S1.

Crystallization and X-Ray structure determination

Crystallization screenings with purified proteins (15 mg/mL in HEPES pH 7.5, 0.15 M NaCl and 0.5 mM TCEP) were initially performed at 20°C using the sitting-drop vapor-diffusion method with sparse matrix crystallization kits. Small needle crystals of the isolated PAPS domain ($hFADS_{355\text{-}553}$) in complex with FAD appeared in 2–3 days in 1.6 M Na/K phosphate, pH 6. Bigger, rod-shaped -crystals could be grown in the same conditions with the addition of 10% DMSO. The crystals of the entire protein lacking the first 12 amino acids ($hFADS_{110\text{-}587}$) were obtained in two days with a solution of 0.1 M MES pH 6.5, 10% PEG 8000 and 10% ethylene glycol as precipitant.

Diffraction data were collected from crystals frozen at 100 K at ID23-2 and ID30B beamlines of the European Synchrotron Radiation Facility (ESRF), in Grenoble DOI: https://doi.org/10.15151/ESRF-ES-925344270 and https://doi.org/10.15151/ESRF-ES-1018420663). The data were processed with the automated pipeline autoPROC[52] and the anisotropy analysis and correction were performed with the STARANISO server.[53] The structure of the PAPS domain-FAD complex was solved by molecular replacement using the software MOLREP,[54] and the coordinates of the *Candida glabrata* FMN adenylyltransferase (PDB ID: 3FWK)[43] as search probe. The model was subjected to multiple rounds of manual rebuilding in COOT[61] and automatic refinement with either Refmac 5[55] and phenix-refine.[56] The ligand and the water molecules were modeled in the residual density identified in the Fo-Fc and 2Fo-Fc maps, and the model was subjected to a final round of refinement with phenix-refine.

The structure of the whole protein was solved by molecular replacement with Phaser[57] using two different search probes: the N-terminal portion of the CinA structure (PDB ID: 4UUW, chain B)[46] for the MPTb-KH domains, and the model of the PAPS domain in complex with FAD for the C-terminal part. After multiple cycles of manual and automated rebuilding with PHENIX AutoBuild,[58] the model was refined with phenix.refine. TLS refinement (1 TLS group per chain), NCS averaging and group isotropic ADP refinement (2 groups per residue) have been used throughout the refinement process.

The stereochemical quality of the final models was assessed with MolProbity.[59] The figures of molecular models were prepared and rendered with PyMOL (http://www.pymol.org) and Chimera.[50] Data collection and refinement statistics are summarized in Table 1.

Isothermal titration Calorimetry (ITC)

ITC measurements were performed with a MicroCal PEAQ-ITC at 25°C. For each experiment, an initial volume of 190 μL of protein (100 μM in 20 HEPES pH 7.5, 0.15 M NaCl, 5 mM $MgCl_2$ and 0.5 mM TCEP) was titrated with 20 injections (2.0 μL each) of 2 mM ligand dissolved in the same buffer, with a stirring rate of 500 rpm. A blank titration (ligand into buffer) was recorded for each experiment and the dilution heats were subtracted to the data. Independent model fitting was used to estimate ΔH and Kd.

Measurements of FAD synthesis and FAD hydrolysis

The rate of FAD synthesis and FAD hydrolysis were measured *in continuo* as in,[25,62] by exploiting the different fluorescence properties of FAD with respect to FMN. Fluorescence time courses (λ excitation at 450 nm; λ emission at 520 nm) were followed at room temperature in an FP-8300 Jasco spectrofluorometer. In each experiment, FMN and FAD fluorescence were calibrated by using

standard solutions whose concentrations (used in the μM range) were calculated by using ε_{450} of 12.2 mM^{-1} cm^{-1} for FMN and 11.3 mM^{-1} cm^{-1} for FAD. Under the experimental condition used here, the specific relative FAD fluorescence coefficient (ϕ_{FAD}) proved to be about ten times lower than those of FMN (ϕ_{FMN}).[62–64] For FAD synthesis rate measurements, purified protein fractions (1–10 μg) were incubated in 50 mM Tris/HCl, pH 7.5, containing 5 mM $MgCl_2$, 2 μM FMN and 100 μM ATP. The rate of FAD synthesis, expressed as nmol FAD · min^{-1} · mg $protein^{-1}$, was calculated from the rate of fluorescence decrease, measured as the tangent to the initial part of the experimental curve by applying the following equation:

$$V_0 = \left[\left(\Delta F_{450/520}/\Delta\phi_{450/520}\right) \cdot Vf\right] \Big/ (t \cdot m)$$

where ΔF is expressed in fluorescence arbitrary units, $\Delta\phi = \phi_{FMN} - \phi_{FAD}$ is expressed as μM^{-1}, Vf is expressed in mL, t is time expressed in min and m is the mass of protein in mg.

For FAD hydrolysis rate measurements, purified protein fractions (3–15 μg) were incubated in 50 mM Tris/HCl, pH 7.5, containing 1 mM $CoCl_2$, 50 mM KCl and 1 μM FAD, unless otherwise indicated. The rate of FAD hydrolysis was expressed as nmol FAD · min-1 · mg protein-1, and was calculated from the rate of fluorescence increase, measured as the tangent to the initial part of the experimental curve as previously described. To fit the experimental data and obtain estimates of kinetic parameters, Grafit software was used.

Molecular docking

The structures of ADP-ribose, FAD and NADH were retrieved from PubChem Database as sdf files, imported into Chimera 1.16 and saved in pdb format. The ligands and protein (consisting of a single dimer of hFADS) were prepared using AutoDock Tools (ADT).[65] Gasteiger charge was assigned and the files were saved in PDBQT format. Blind molecular docking was performed with AutoDock Vina v.1.1.2.[51] The grid size covering the whole dimer was set to 80 × 80 × 82 Å (x, y, and z) with spacing 1. Each docking experiment was repeated three times, resulting in a total of 27 poses per ligand. After inspection in Chimera, the pose with the lowest energy (*Z* score) was selected for each ligand.

QUANTIFICATION AND STATISTICAL ANALYSIS

X-ray crystallography data collection and refinement statistics are listed in Table 1. Details of the programs used can be found in both the key resources table and method details section.

The rates of FAD synthesis and hydrolysis displayed in Figure 1 are given as mean ± SD of two independent experiments. The kinetic parameters were obtained fitting the data according to the Michaelis–Menten equation with Grafit 5.0.13 software and reported in Table S1 as mean ± SD (n = 2).

Independent sites model fitting of ITC data was used to derive the thermodynamic parameters reported in the legend of Table S3 as descried in Method details. Data were fitted with the MicroCal PEAQ-ITC Analysis Software.